



# Low Temperature CO Oxidation Over Highly Active Gold Nanoparticles Supported on Reduced Graphene Oxide@Mg-BTC Nanocomposite

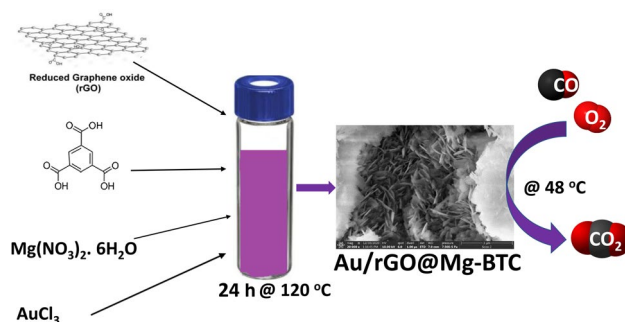
Hatem M. Altass<sup>1</sup> · Saleh A. Ahmed<sup>1,2</sup> · Reda S. Salama<sup>3</sup> · Ziad Moussa<sup>4</sup> · Rabab S. Jassas<sup>5</sup> · Reem I. Alsantali<sup>6</sup> · Munirah M. Al-Rooqi<sup>1</sup> · Amr A. Ibrahim<sup>7</sup> · Menna A. Khder<sup>7</sup> · Moataz Morad<sup>1</sup> · Awad I. Ahmed<sup>7</sup> · Abdelrahman S. Khder<sup>1,7</sup>

Received: 16 February 2022 / Accepted: 13 April 2022 / Published online: 9 May 2022  
© The Author(s), under exclusive licence to Springer Science+Business Media, LLC, part of Springer Nature 2022

## Abstract

In this study, gold nanoparticles (Au NPs) were successfully supported on reduced graphene oxide (rGO) and Mg-BTC in one pot under solvothermal conditions. The catalysts contain different amounts of Au NPs started from 1.0 up to 7.0 wt%. All of these catalysts were characterized by different techniques such as XRD, BET, TEM, SEM, XPS and TGA. The results exposed that the Au NPs were extremely dispersed on the surface of rGO@Mg-BTC catalyst as displayed in TEM and SEM images. Moreover, the XPS study showed proved the existence of both Au<sup>0</sup>, Au<sup>1+</sup> and different surface oxygen species on the catalyst surface. CO oxidation as a model reaction was then used to evaluate the catalytic activity of the as-synthesized composites. The results showed the main and vital role of Au NPs, their distribution and oxidation state in the oxidation of CO gas at low temperatures. Where the study proved the presence of both Au<sup>0</sup> particles and surface oxygen species on the surface increases the rate of adsorption and oxidation of CO gas. The study also showed that these catalysts prepared in one pot have outstanding stability with the possibility of reuse up to ten times without losing their catalytic activity. Which makes these catalysts have a high efficiency in protecting the environment from the poisonous CO gas.

## Graphical Abstract



**Keywords** CO oxidation · Au nanoparticles · rGO · Mg-BTC · Nanocomposites

## 1 Introduction

Currently, there is a rapid progress in industrial plants and vehicles which produce humungous amounts of waste gases that are very toxic to the human health and environment. One of the most toxic gases that emitted from devices with combustion process is carbon monoxide (CO), which does not react with the substances directly, but it binds to hemoglobin

✉ Saleh A. Ahmed  
saahmed@uqu.edu.sa; saleh\_63@hotmail.com

✉ Abdelrahman S. Khder  
askhder@uqu.edu.sa; askhder2244@yahoo.com

Extended author information available on the last page of the article

directly and replace the oxygen. Therefore, their removal is a crucial task of today, while keeps still a great challenge [1–3]. One of the most significant processes for air purification is CO oxidation at lower temperature, which depends on the oxidation of CO to CO<sub>2</sub> [4–7]. CO oxidation at lower temperature received much consideration because of its significant applications in numerous fields such as preferential oxidations (PROX) in hydrogen-rich streams, close-cycle CO<sub>2</sub> lasers, automobile exhaust emission control, respiratory protection and indoor air purification and CO gas sensors [1, 8]. Lately, the technology option has found a new application for removing trace CO from confined spaces including coal mine refuge chambers, space-crafts and submarines [9].

Mesoporous materials are widely as catalyst and/or support in many applications [10–13]. One of the most highly porous crystalline materials in the last few years is metal–organic frameworks (MOFs), which constructed from polyfunctional organic linkers and metallic clusters or metal ions [14–19]. MOFs have attracted considerable attention due to their very high surface area, tunable pore sizes, modifiable surface properties, well-defined channels or cavities and remarkable permanent porosity [20, 21]. These physico-chemical properties offer numerous applications in different fields including heterogeneous catalysis, gas storage media, gas separation, dye and metal removal, chemical sensors and batteries, drug carriers and biomedical imaging [22–29]. Several approaches were used to modify and increase the catalytic sites or unsaturated coordination sites of metal organic frameworks through surface modifications by different active species including transition metals or noble metals nanoparticles [30–32]. These catalytic activities of metal organic frameworks have been examined for liquid-phase reactions such as oxygen reduction reactions in fuel cells [33], photocatalytic hydrogen production [34], organic transformations reactions [21] and cyanosilylation, isomerization, polymerization and hydrogenation reactions [35]. Otherwise, only few gas–solid reactions using metal organic framework have been verified in CO oxidation [36, 37]. One of the most novel and unique MOFs is Mg-BTC, which constructed from magnesium metal or cluster bonded with 1,3,5 benzene tricarboxylic acid (BTC) as a linker. Mg-MOF has potential application including drug delivery, catalysis and adsorption [38, 39].

One of the most important supports that used as catalysts is reduced graphene oxides because of their unique structure, intrinsic properties and ability for surface modification [40]. Graphene-supported over different metal oxides of nanoparticles such as TiO<sub>2</sub> [41], CeO<sub>2</sub> [42], MnO<sub>2</sub> [43], Pd [44] and Pt [45] catalysts have been lately testified on numerous catalytic reactions and showed excellent activities. Nobel metals supported on different materials exhibited excellent behavior towards CO oxidation. Gold (Au) nanoparticles is one of the most important transition Nobel metal that used to

improve CO oxidation at lower temperatures [46, 47]. This is due to unexpected catalytic activities when the particles size is decreased to nanometer scale, low-coordinated Au atoms, charge transfer and Au oxidation state [46–49].

In current work, an attempt was completed to enhance the ability of Mg-MOF toward catalytic CO oxidation reaction by modification with reduced graphene oxide and different weight contents of gold nanoparticles. Magnesium-based metal organic framework (Mg-BTC) was successfully synthesized from the interaction between trismic acid (BTC) as a linker and magnesium metal clusters as a node. Our tactic is to improve the catalytic activity of the prepared MOF in presence of graphene oxide and gold nanoparticles through one pot solvothermal synthesis method. The as-synthesized composites (*x* wt. Au/rGO@Mg-BTC) were characterized using numerous techniques such as XRD, BET, TEM, SEM and XPS. The catalytic activities of the prepared composites were testified toward CO oxidation and the stability of these composites were investigated.

## 2 Experimental

### 2.1 Preparation of the Catalysts

Firstly, reduced graphene oxide (rGO) was prepared through modified Hummer method as explained in detail in our earlier work [40]. After that, 1.0 wt% rGO@Mg-BTC were synthesis by the same approach that used in the preparation of Mg-BTC but in the presence of reduced graphene oxide [38]. Typically, a stock solution consists 30 ml dimethylformamide (DMF), 40 ml ethanol and 30 ml deionized water was prepared. Then calculated amount of graphene oxide was dispersed and sonicated in 30 ml of the stock solution for 1 h (solution A). On the other hand, 1.314 g of magnesium nitrate and 0.708 g of trismic acid (H<sub>3</sub>BTC) were completely dissolved in 30 ml DMF (Solution B). After that, the two solutions (A and B) were mixed by stirring for 30 min. then transferred to the Teflon lined autoclave and heated to 120 °C for 24 h. The resulting composite was separated by centrifuge, washed three times with DMF followed by ethanol and dried at 100 °C overnight. For the preparation of gold NPs with different amounts (1.0, 3.0, 5.0 and 7.0 wt%) supported on rGO@Mg-BTC, calculated volumes of gold(III) chloride hydrate solution were added during the preparation of rGO@Mg-BTC composites as shown before.

### 2.2 Characterization

XRD patterns of all prepared catalyst were examined using X'Pert Philips PW150 diffractometer, which operated at 40 kV and current value 45 mA using Cu K $\alpha$  ( $\lambda=0.15417$  nm). All the prepared catalysts were scanned

from  $2\theta$  equal  $10^\circ$  to  $80^\circ$  to clarify the crystallinity. The average pore diameter, pore size distribution and specific surface area of the prepared catalysts were calculated from  $N_2$  adsorption/desorption studies at  $-196^\circ\text{C}$  using Quanta Chrome NOVA touch LX<sup>4</sup> instrument. The topography and morphology of the prepared samples were investigated using transmission electron microscopy (TEM, JEOL JEM-2100) and scanning electron microscope (SEM, Jeol JSM-6510LV). The chemical structure and oxidation states of the catalysts were examined through XPS measurement using thermo ESCALAB 250Xi spectrometer with a monochromatic Al K $\alpha$  (1486.6 eV) radiation. The thermal stability of the composites was measured using Shimadzu TGA-50/50H thermogravimetric analyzer at range of  $30\text{--}800^\circ\text{C}$  with a temperature rate of  $20^\circ\text{C min}^{-1}$  in air.

### 2.3 Catalytic Activity Test

CO oxidation studies were examined through the following: firstly, 0.7 g of the prepared samples were treated in helium gas flow at  $110^\circ\text{C}$  for 15 min to remove all adsorbed impurities and moisture on its surfaces. Then, the catalyst was moved to a tubular quartz reactor with an inner diameter (i.d) equal 6 mm then transferred to Thermolyne 2100 programmable tube furnace reactor. Then, a gas mixture containing 76.0 wt% Argon, 20.0 wt% oxygen and 4.0 wt% carbon monoxide was passed over the catalyst with  $50\text{ cc min}^{-1}$  flow rate and the temperature of the prepared catalyst was increased with a heat rate  $5^\circ\text{C min}^{-1}$  from room temperature till complete oxidation of CO. The conversion of CO to  $\text{CO}_2$  was detected by an infrared gas analyzer (MGA 3000 multi-gas analyzer, ADC).

## 3 Results and Discussion

### 3.1 X-Ray Diffraction Pattern (XRD)

The XRD patterns of pure and modified Mg-BTC with a different weight percentage of gold NPs (1.0, 5.0, 7.0 wt%) are displayed in Fig. 1. The XRD pattern of the support (Mg-BTC) obviously shows the presence of characteristic peaks at  $2\theta$  equal  $24.9^\circ$ ,  $36.9^\circ$  and  $50.4^\circ$  which are in good agreement with the previously reported patterns (CCDC 768995) revealing that the Mg-BTC metal organic framework was successfully synthesized and have excellent crystallinity [39, 50]. After modification with GO and Au NPs, There are other peaks were observed at  $2\theta$  equal  $40.1^\circ$ ,  $46.5^\circ$ ,  $66.2^\circ$  which are slightly matched with face-centered-cubic Au (JCPDS No.001-1172) [48] with some shifting at  $2\theta$  equal  $40.1^\circ$  compared with referenced Au (111) peak ( $38.2^\circ$ ). This shifting could be due to the existence of rGO and Mg-BTC in the same framework [51]. Also, the figure displayed that

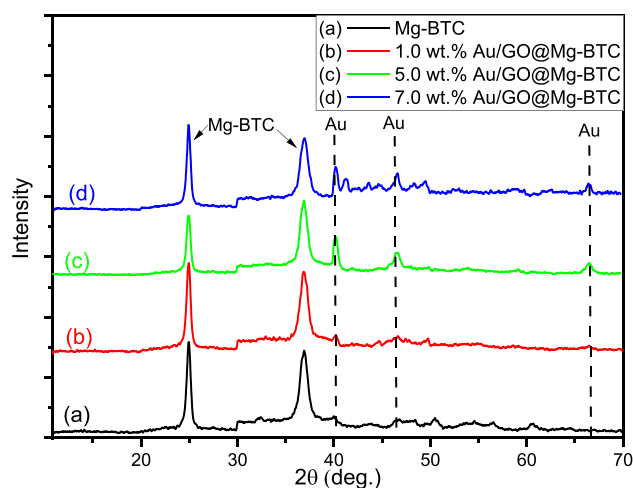


Fig. 1 XRD Patterns of (a) Mg-BTC, (b) 1.0 wt%, (c) 5.0 wt% and (d) 7.0 wt% Au/GO@Mg-BTC

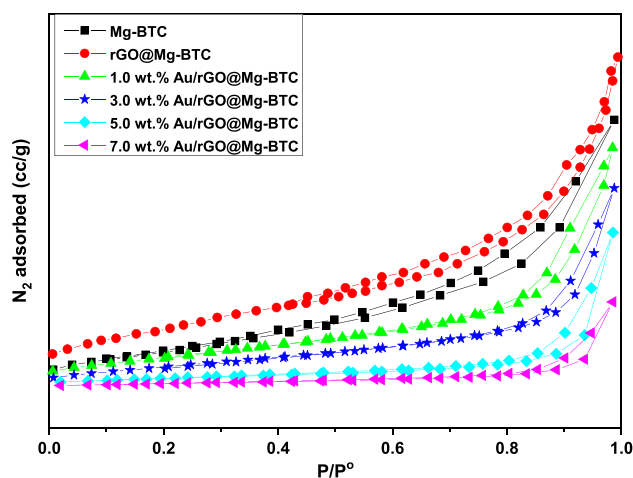


Fig. 2  $N_2$  adsorption–desorption isotherms of pure and modified Mg-BTC with rGO and Au NPs

the intensity related to Au NPs was increased with increasing the amount of gold on the surface of Mg-BTC. The XRD results revealed that the Mg-BTC keeps its structure stable even after modification with rGO and different amounts of Au NPs, and all Au NPs are successfully dispersed homogeneously and finely on the surface of rGO@Mg-BTC nanocomposite.

### 3.2 Surface Area Measurements

The textural properties of the prepared composites (Mg-BTC and x wt% Au/rGO@Mg-BTC) were investigated through  $N_2$  physisorption studies, the results are displayed in Fig. 2. The figure reveals that all the as-synthesized composites have a type-II isotherms with H3 hysteresis loop according

to the IUPAC classification which prove that the prepared samples contain mesoporous nature and the presence of a hysteresis loop at high relative pressure ( $P/P^0$ ) related to the stacking particles in the holes [52–54]. Surface area ( $S_{\text{BET}}$ ) and pore structure parameters of the as-synthesized catalysts were displayed in Table 1. The table showed that  $S_{\text{BET}}$  of Mg-BTC was raised from 731 to 781  $\text{m}^2 \text{g}^{-1}$  after modification with reduced graphene oxides (rGO), which may be due to the attachment of rGO to the surface of Cu-BTC to form a more porous structure [4]. On the other hand, when rGO@Mg-BTC composite was modified with different weight contents of gold nanoparticles, the surface area decreased until it reached 363  $\text{m}^2 \text{g}^{-1}$  at 7 wt% Au/rGO@Mg-BTC. This decrease in surface area may be due to the stacking of gold NPs inside the pores of rGO@Cu-BTC crystals [4].

The pore size distributions of the prepared catalysts were measured using a BJH method and the results are shown in Fig. 3. The figure indicates a broad distribution in the mesoporous range of 2–50 nm for all the prepared nanocomposites. Pure Mg-BTC displayed uniform and narrow pore size distributions centered at 6.3 nm, which decreased with increasing rGO to 5.5 nm and there is a new peak observed at 2.7 nm in the case of rGO@Mg-BTC. After modification with Au NPs, the main peak was decreased to a lower pore diameter. Also, the intensity of the main peak was decreased which could be attributed to the low surface area.

### 3.3 SEM Images

The morphology of pure and modified Mg-BTC catalysts with Au NPs were investigated through scanning electron microscopy (SEM) images and displayed in Fig. 4. According to Fig. 4a, the Mg-BTC catalyst displayed 2D nanosheets like structure, when the rGO was inserted the nanosheets structure was changed to an irregular sheet like structure (Fig. 4b). After modification with gold nanoparticles, there are different spherical nanoparticles were observed in the nanosheets like structure (Fig. 4c, d). The figures displayed that the spherical nanoparticles were increased with the increase in the contents of Au NPs, which reveals that Au NPs were successfully dispersed on the surface of rGO@Mg-BTC.

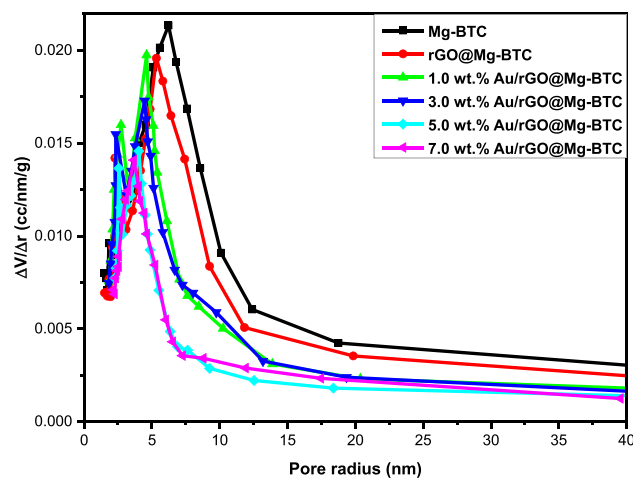


**Fig. 3** Pore size distribution of pure and modified Mg-BTC with rGO and Au NPs

### 3.4 TEM Images

To clearly prove the dispersion of Au NPs on rGO@Mg-BTC, TEM images of Mg-BTC, rGO@Mg-BTC, 3.0 wt% and 7.0 wt% Au/rGO@Mg-BTC were recorded. According to Fig. 5, Mg-BTC catalyst possesses a disordered sheets like structure even after the addition of rGO (Fig. 5a, b). After modification with a different weight percentage of Au NPs, it can be found that nanosized spherical Au NPs were well dispersed on the surface of rGO@Mg-BTC and the number of these nanoparticles was increased with increasing the amount of Au NPs loading (Fig. 5c–e). According to the Au nanoparticle size distribution histograms (Fig. 1S), the average sizes of Au nanoparticles were found to be 14.6, 15.1 and 15.9 nm for 3.0, 5.0 and 7.0 wt% Au/rGO@Mg-BTC respectively, which displayed that the average crystal size was increased by increasing the contents of gold.

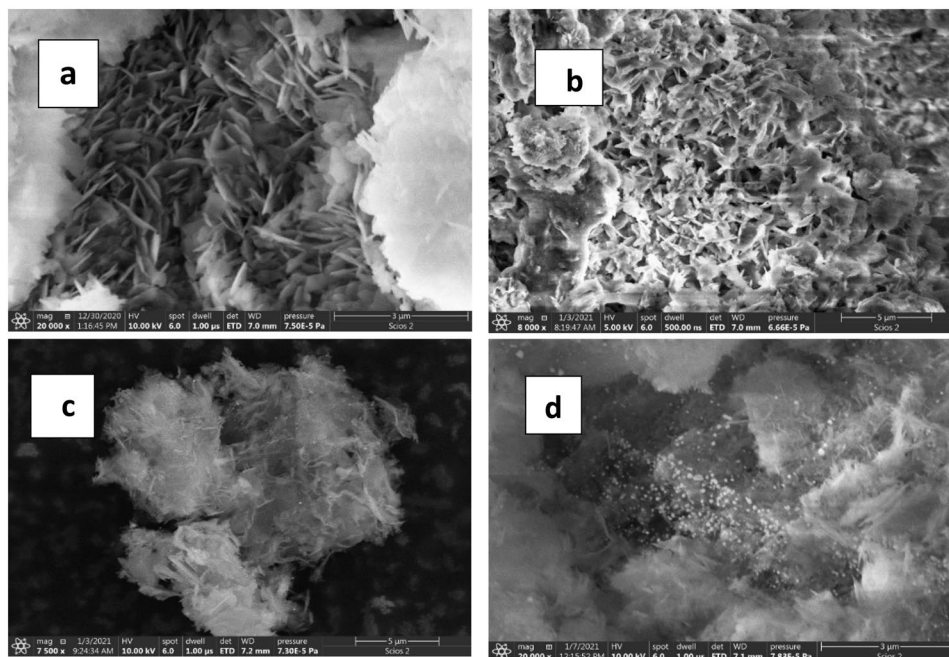
### 3.5 XPS Measurements

X-ray photoelectron spectroscopy (XPS) was used to investigate the surface composition and chemical state of the prepared catalysts. As displayed in Fig. 6. Figure 6a

**Table 1** surface structure parameters and catalytic activity of the as-synthesized catalysts

Sample	BET surface area ( $\text{m}^2 \text{g}^{-1}$ )	Pore volume ( $\text{cm}^3 \text{g}^{-1}$ )	Pore diameter (nm)	CO conversion	
				$T_{50}$ ( $^{\circ}\text{C}$ )	$T_{100}$ ( $^{\circ}\text{C}$ )
Mg-BTC	731	0.68	6.2	209	222
rGO@Mg-BTC	780	0.73	5.4	205	213
1.0 wt% Au/rGO@Mg-BTC	690	0.63	4.7	113	138
3.0 wt% Au/rGO@Cu-BTC	642	0.54	4.5	64	76
5.0 wt% Au/rGO@Cu-BTC	488	0.42	4.1	39	48
7.0 wt% Au/rGO@Cu-BTC	363	0.39	3.5	81	126

**Fig. 4** SEM images of **a** Mg-BTC, **b** rGO@Mg-BTC, **c** 3.0 wt% Au/rGO@Mg-BTC and **d** 7.0 wt% Au/rGO@Mg-BTC



showed the survey spectra of 5.0 wt% of gold supported on rGO@Mg-BTC, which showed four main peaks (gold (Au), Magnesium (Mg), Oxygen (O) and carbon (C)) observed at binding energy values of 90.4 (Au4f), 1302.5 (Mg1s), 532.5 (O1s) and 283.9 eV (C1s). From the survey spectra, the weight percentage of each element was found to be that Au4f has 4.5 wt%, Mg1s has 14.6 wt%, O1s has 34.8 wt% and C1s has 46.1 wt%. These data proved that the actual composition of 5.0 wt% Au/rGO@Mg-BTC is very close to the theoretical value. Additionally, the high resolution XPS spectrum in Fig. 6b was fitted to two peaks. The two peaks located at 83.7 eV and 88.6 eV are attributed to Au 4f7/2 and 4f5/2, which exhibit a negative shift of 0.3 eV and 1.0 eV in comparison to 84.0 and 87.6 eV of the bulk Au. It is generally believed that this shift is caused by electron transfer from plasmonic Au to rGO@Mg-BTC that may be due to the strong electronic interaction between the Au and the support, which has also been reported by other research groups [55–58]. On the other hand, The XPS spectrum of C1s was displayed in Fig. 6c, in which there are four main peaks observed at 284.6, 286.2, 288.1, 289.6 eV that are related to C–C/C=C and C–H bond, C–O and C=O, respectively, demonstrating the existence of BTC [5]. Also, Fig. 6d showed three peaks positioned at 529.6 eV (carbonyl (C=O)), 531.5 eV (carboxylic (O–C=O)) and 533.3 eV (Hydroxyl (H–O)) [59]. The high-resolution spectrum of Mg1s spectrum displayed two peaks positioned at about 1303.7 and 1304.9 eV, which are attributed to Mg–O and Mg–C bonding, respectively (Fig. 6e) [60]. The oxidation state of the gold supported on rGO@Mg-BTC was confirmed.

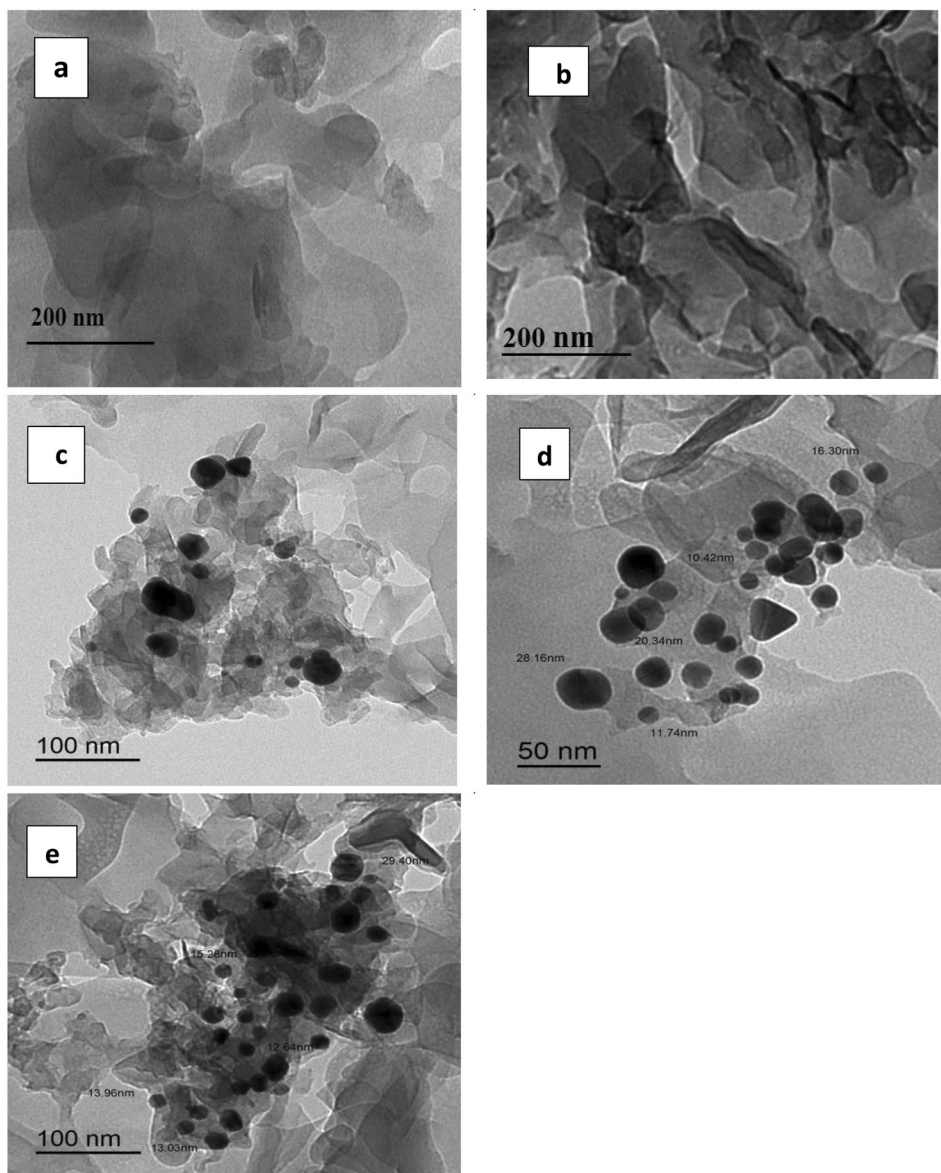
### 3.6 TGA Analysis

Thermal gravimetric analysis (TGA) was introduced to measure the thermal stability of the as-synthesized catalysts as displayed in Fig. 7. The figure displayed that TGA curve of the prepared catalysts has a thermal behavior with two separated regions. The first region is attributed to the evaporation of the adsorbed water molecules and the second one is related to the decomposition of the structure. From Fig. 7a, Mg-BTC catalyst starts to decompose from 105 to 145 °C with weight loss 10.6% (evaporation of adsorbed water). Then, decomposed again at temperature ranged from 282 to 371 °C with weight loss 33.1% (decomposition of the structure). While rGO@Mg-BTC (Fig. 7b) showed 7.9% weight loss at the first region and 27.5% weight loss at temperature ranged from 330 to 440 °C. From these data, addition of rGO over Mg-BTC could enhance the thermal stability of Mg-BTC due to the good stability of rGO after 300 °C. After addition of Au NPs, the thermal stability of Mg-BTC was improved due to the existence of gold nanoparticles as metals [4, 61].

### 3.7 Catalytic Performance

The catalytic performance of the as-synthesized gold nanoparticles supported on rGO@Mg-BTC catalysts toward CO oxidation are shown in Fig. 8 and their corresponding light-off temperatures at 50% ( $T_{50}$ ) and 100% ( $T_{100}$ ) CO conversions are cited in Table 1. According to Fig. 8a, the oxidation of CO over pure Mg-BTC was started at around 200 °C where  $T_{50}$  and  $T_{100}$  are found to be at 209 and 222 °C

**Fig. 5** TEM images of **a** Mg-BTC, **b** rGO@Mg-BTC, **c** 3.0 wt% Au/rGO@Mg-BTC, **d** 5.0 wt% Au/rGO@Mg-BTC and **e** 7.0 wt% Au/rGO@Mg-BTC



respectively. The activity of pure Mg-BTC may be attributed to the support's porous structure ( $S_{\text{BET}}$ ,  $730.9 \text{ m}^2 \text{ g}^{-1}$ ;  $V_{\text{tot}}$ ,  $0.68 \text{ cm}^3 \text{ g}^{-1}$ ) having a large amount of surface defects, that could adsorb and activate CO and  $\text{O}_2$ . Sadri et al. [59] did not observe any catalytic activity of the Mg-BTC up to  $200 \text{ }^\circ\text{C}$ , which is consistent with these results. Moreover, the modification of Mg-BTC with 1 wt% rGO was accompanied by a slight enhancement of the catalytic performance where  $T_{50}$  and  $T_{100}$  are shifted to  $205$  and  $213 \text{ }^\circ\text{C}$  (Fig. 8b, Table 1). Interestingly, when rGO@Mg-BTC nanocomposite was modified with Au NPs remarkable enhancement of the catalytic performance was observed as shown in Fig. 8c–f. This outstanding behavior of Au supported catalysts may explain the critical role played by Au NPs. Furthermore, the increase of AuNPs content from 1 wt% up to 5 wt% was accompanied by the gradual shift of  $T_{50}$  and  $T_{100}$  to lower

temperatures as observed in Table 1. These results indicated that the 5.0 wt% Au/rGO@Mg-BTC sample exhibited the best catalytic performance toward CO oxidation ( $T_{50} = 39 \text{ }^\circ\text{C}$  and  $T_{100} = 48 \text{ }^\circ\text{C}$ ) compared to the other catalysts. Conversely, at a higher Au NPs loading (7 wt%) notable decrease in the activity was observed and the values of  $T_{50}$  and  $T_{100}$  were shifted to  $81$  and  $126 \text{ }^\circ\text{C}$ , respectively. This decrease in catalytic activity was accompanied by a notable decrease in the surface area which and the agglomeration of gold NPs on the support as evident by XRD and TEM images.

The mechanism of CO oxidation was previously discussed by many authors and it was reported that the oxidation mechanism may be affected by many factors such as the dispersion, particle size and oxidation state of the Nobel metal as well as active oxygen supplied by the support [62–65]. In the present work, it seems that the CO oxidation

**Fig. 6** XPS spectra of 5.0 wt% Au/rGO@Mg-BTC: **a** survey spectra, **b** Au4f spectrum, **c** C1s spectrum, **d** O1s spectrum and **e** Mg1s spectrum

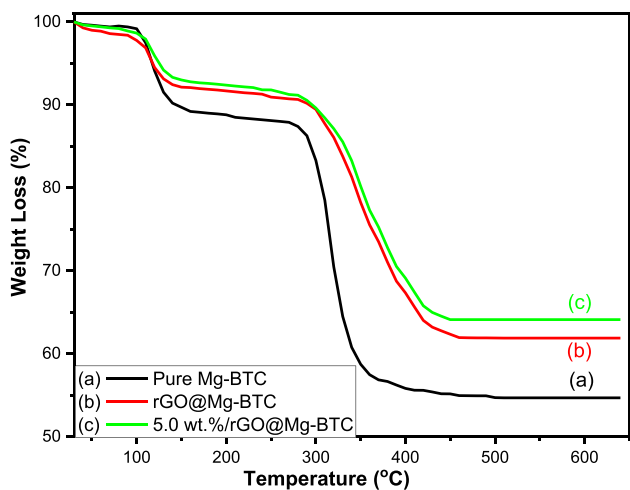
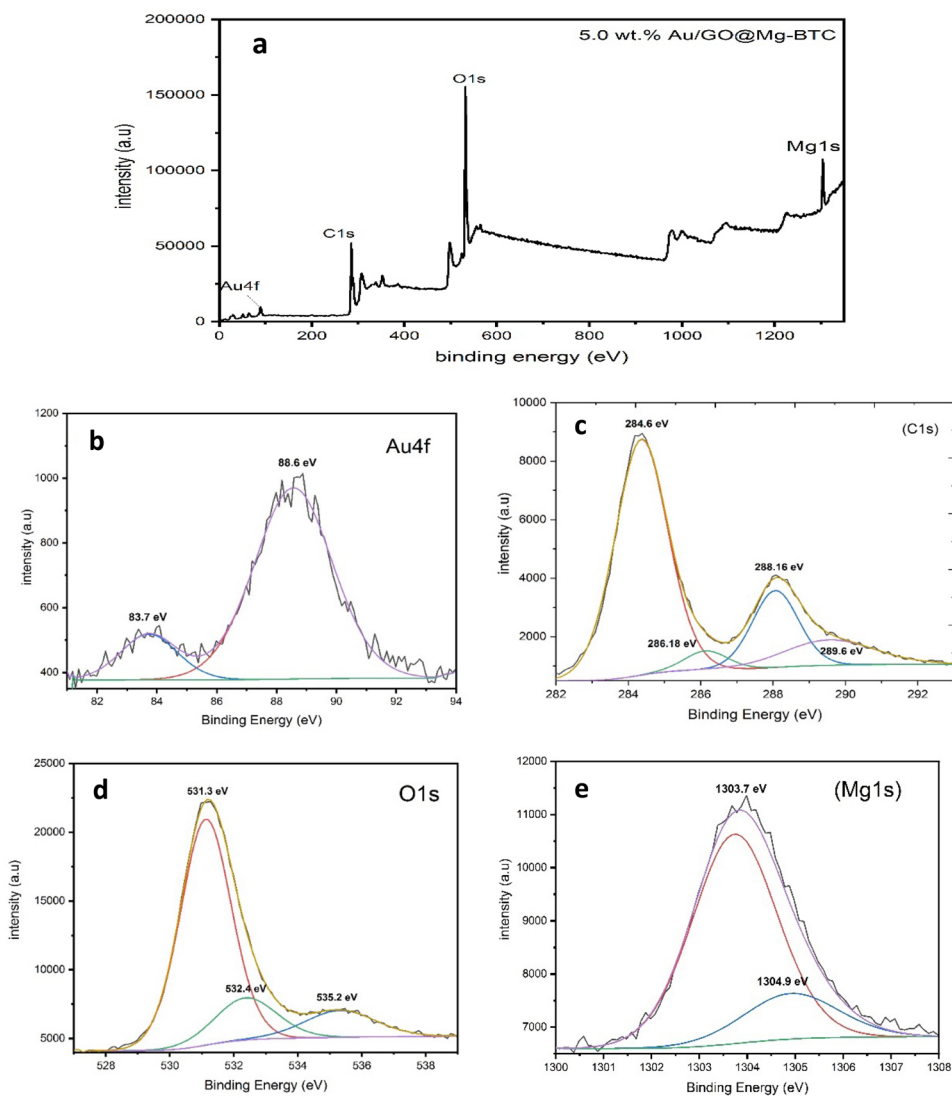


**Fig. 7** TGA Curves of **a** pure Mg-BTC, **b** rGO@Mg-BTC and **c** 5.0 wt% Au/rGO@Mg-BTC

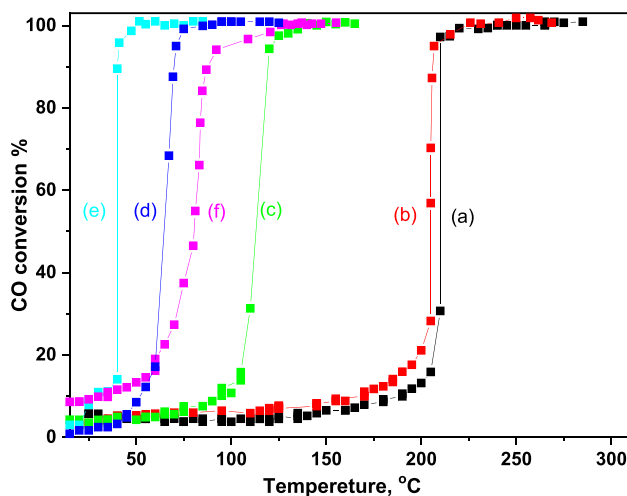


**Fig. 8** CO conversion as a function of temperature of (a) pure Mg-BTC, (b) rGO@Mg-BTC, (c) 1.0 wt%, (d) 3.0 wt%, (e) 5.0 wt%, (f) 7.0 wt% Au/rGO@Mg-BTC

mechanism is through the adsorption of CO gas on the surface of Au<sup>0</sup>, followed by the oxidation process by the active oxygen supplied by the support. This idea may be supported by XPS results which proved the existence of Au<sup>0</sup> as well as different forms of surface oxygen species on the support surface. Thus, when the dispersion of Au NPs is optimum as in case of 5 wt% Au/rGO@Mg-BTC catalyst (as evident by SEM and TEM images), the number of active centers of Au<sup>0</sup> NPs exposed to the surface increases, which is accompanied by an increase in the rate of adsorption and oxidation of CO gas. Moreover, the higher loading of Au NPs (7 wt%) is accompanied by the agglomeration and grow of some populations of Au NPs on the surface, which reduces the number of active centers and thus reduces both the rate of adsorption and oxidation of CO gas.

The effect of the catalyst weight on the oxidation of CO was investigated over some selected catalysts, and the observed results are presented in Fig. 9. The results demonstrate that by increasing the catalyst weight from 0.01 to 0.07 g, the 100% conversion temperature of CO oxidation was shifted to lower values. This expected shift of the 100% CO conversion to lower temperatures may be attributed to increasing the number of active sites as the catalyst weight is increased. Additionally, some slight changes in the 100% CO conversion temperatures were observed when the catalyst weight was increased from 0.07 to 0.1 g. According to these results, the optimum catalyst weight that used in all CO oxidation experiments was chosen to be 0.07 g.

The reusability test was investigated over some selected catalysts, in this experiment 0.07 g of each catalyst was used in ten consecutive runs without any further treatment, the results were collected and displayed in Fig. 10. As it can be seen, the catalysts exhibited excellent reusability where the 100% CO conversion temperatures ( $T_{100}$ ) were slightly

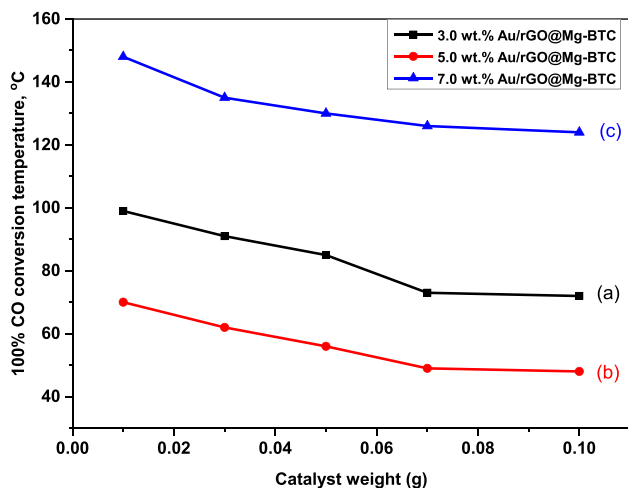


**Fig. 9** Effect the catalyst weight on  $T_{100}$  over (a) 3.0 wt%, (b) 5.0 wt% and (c) 7.0 wt% Au/rGO@Mg-BTC

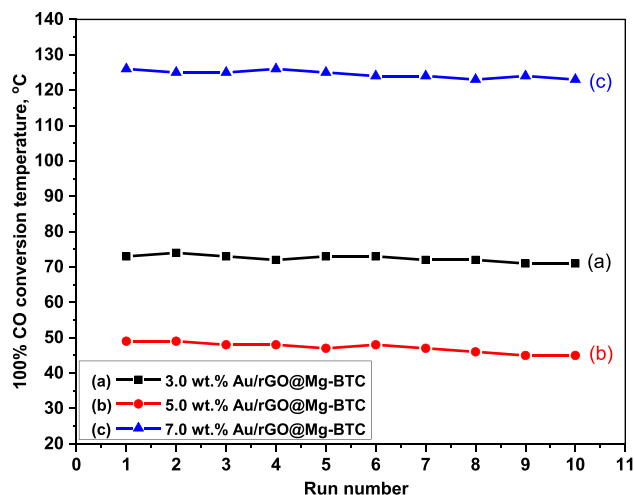


**Fig. 10** Reusability test according to  $T_{100}$  value over (a) 3.0 wt%, (b) 5.0 wt% and (c) 7.0 wt% Au/rGO@Mg-BTC

changed even after 10 successive runs. This could be due to the good dispersion of Au NPs and high surface area of the as-synthesized catalysts that guarantying good stability and high catalytic activity. Also, the stability of the catalyst was measured by comparing the catalytic activity of 5.0 wt% Au/rGO@Mg-BTC with the same percentage of gold on reduced graphene oxide (5.0 wt% Au/rGO) and on Mg-BTC (5.0 wt% Au/Mg-BTC) as displayed in Fig. 2S. The results showed that 5.0 wt% Au/rGO@Mg-BTC sample still exhibited the best catalytic performance toward CO oxidation ( $T_{50}=39$  °C and  $T_{100}=48$  °C) compared 5.0 wt% Au/rGO ( $T_{50}=106$  °C and  $T_{100}=113$  °C) and 5.0 wt% Au/Mg-BTC ( $T_{50}=114$  °C and  $T_{100}=127$  °C). This enhancement of the catalytic performance in the presence of rGO could be due to graphene-based materials with functional groups and defects of different nature, play one of the major roles in catalysis, by activating oxygen dissociation and electron transfer between gas molecules and catalysts surface [66, 67]. Moreover, plays a vital role in the dispersion of Au NPs on the catalyst surface, resulting in higher number of Au active sites compared with the catalyst without rGO [67, 68].

The catalytic activity toward CO oxidation over Au NPs catalyst supported on different supports was examined in numerous previous literatures [69–71]. So, by comparing our recent work with previously reported Au NPs supported catalysts (Table 1S), we found that 5.0 wt% Au/rGO@Mg-BTC act as an excellent catalyst toward CO oxidation by achieving the value of 100% CO conversion at lower temperature.



## 4 Conclusion

In summary, we have developed a general, facile and effective method based on solvothermal approach for the insertion of Au NPs within rGO@Mg-BTC in one step method. The properties of the synthesized catalysts were fully studied by numerous characterization techniques. The results showed that the prepared catalysts provided enough surface area ( $S_{\text{BET}}$ ) and display excellent dispersion of Au NPs on the surface of rGO@Mg-BTC composite. The results also showed the presence of both Au<sup>0</sup> and Au<sup>1+</sup> on the surface. The catalytic performance of the catalysts was tested in the CO oxidation reaction. The 5wt% Au/rGO@Mg-BTC catalyst showed the highest activity towards CO oxidation with 100% CO conversion at 48 °C. Both surface dispersion of Au NPs and surface oxygen species were found to be the main factors affecting the adsorption and oxidation rates of CO gas. Additionally, the prepared catalysts showed an exceptional stability for ten runs without a significant loss in the catalytic activity and stability according to reusability test. The preparation method used in this work added new and distinctive properties to Mg-BTC, which facilitate the use of such materials with high efficiency in various fields, including oxidation reactions.

**Supplementary Information** The online version contains supplementary material available at <https://doi.org/10.1007/s10562-022-04026-y>.

**Acknowledgements** The authors would like to acknowledge the Deanship of Scientific Research at Umm Al-Qura University, for supporting this work by Grant Code: 22UQU4330066DSR01. The authors would like to extend their sincere appreciation to Taif University Researchers Supporting Project Number (TURSP-2020/312), Taif University, Taif, Saudi Arabia. Dr. Ziad Moussa is grateful to the United Arab Emirates University (UAEU) of Al-Ain and to the Research Office for supporting the research developed in his laboratory (Grant No. G00003291).

**Data Availability** All data generated or analyzed during this study are included in this published article (and its supplementary information files).

## Declarations

**Conflict of interest** We declare that we do not have any commercial or associative interest that represents a conflict of interest in connection with the work submitted.

## References


- Esquinas-Requena JL, Lozoya-Moreno S, García-Nogueras I et al (2020) La anemia aumenta el riesgo de mortalidad debido a fragilidad y discapacidad en mayores: Estudio FRADEA. *Atención Primaria* 52:452–461
- Fouad OA, Khder AERS, Dai Q et al (2011) Structural and catalytic properties of ZnO and Al<sub>2</sub>O<sub>3</sub> nanostructures loaded with metal nanoparticles. *J Nanopart Res* 13:7075–7083
- Khder AS, Ahmed SA, Altass HM et al (2020) CO oxidation over noble metals supported on copper oxide: effect of Cu<sup>+</sup>/Cu<sup>2+</sup> ratio. *J Mater Res Technol* 9:14200–14211
- Altass HM, Morad M, Khder AE-RS et al (2021) Enhanced catalytic activity for CO oxidation by highly active Pd nanoparticles supported on reduced graphene oxide/copper metal organic framework. *J Taiwan Inst Chem Eng* 128:194–208
- Salama RS, Mannaa MA, Altass HM et al (2021) Palladium supported on mixed-metal-organic framework (Co-Mn-MOF-74) for efficient catalytic oxidation of CO. *RSC Adv* 11:4318–4326
- Jassas RS, Alsimaree AA, Ahmed SA et al (2021) Enhanced catalytic activity for CO oxidation by highly active Pd nanoparticles supported on reduced graphene oxide/copper metal organic framework. *J Taiwan Inst Chem Eng* 128:194–208
- Salama RS, El-Sayed ESM, El-Bahy SM et al (2021) Silver nanoparticles supported on UiO-66 (Zr): as an efficient and recyclable heterogeneous catalyst and efficient adsorbent for removal of indigo carmine. *Colloids Surf A* 626:127089
- Abd El Rahman SK, Ashour SS, Altass HM et al (2016) Pd nanoparticles supported on iron oxide nanorods for CO oxidation: effect of preparation method. *J Environ Chem Eng* 4:4794–4800
- Sribnik F, Birbara PJ, Faszczka JJ et al (1990) Smoke and contaminant removal system for space station. *SAE Trans* 99:1145–1153
- Ibrahim AA, Salama RS, El-Hakam SA et al (2021) Synthesis of 12-tungstophosphoric acid supported on Zr/MCM-41 composite with excellent heterogeneous catalyst and promising adsorbent of methylene blue. *Colloids Surf A* 631:127753
- El-Hakam SA, El-Khouly AA, Khder AS (1999) Effect of thermal treatment on various characteristics of nickel/aluminum phosphate catalysts. *Appl Catal A* 185:247–257
- Khder AERS, Ahmed SA, Khairou KS et al (2018) Competent, selective and high yield of 7-hydroxy-4-methyl coumarin over sulfonated mesoporous silica as solid acid catalysts. *J Porous Mater* 25:1–13
- Al-Shehri B, Altass HM, Ashour SS et al (2020) Enhancement the photocatalytic performance of semiconductors through composite formation with Eu-TUD-1. *Optik (Stuttgart)* 202:163522
- Salama RS, El-Hakam SA, Samra SE et al (2018) Adsorption, equilibrium and kinetic studies on the removal of methyl orange dye from aqueous solution by using of copper metal organic framework (Cu-BDC). *Int J Mod Chem* 10:195–207
- El-Dafrawy SM, Salama RS, El-Hakam SA et al (2020) Bimetal-organic frameworks (Cu<sub>x</sub>-Cr<sub>100-x</sub>-MOF) as a stable and efficient catalyst for synthesis of 3,4-dihydropyrimidin-2-one and 14-phenyl-14H-dibenzo [a, j] xanthene. *J Mater Res Technol* 9:1998–2008
- Salama RS, Hassan SM, Ahmed AI et al (2020) The role of PMA in enhancing the surface acidity and catalytic activity of a bimetallic Cr-Mg-MOF and its applications for synthesis of coumarin and dihydropyrimidinone derivatives. *RSC Adv* 10:21115–21128
- El-Hakam SA, Ibrahim AA, Elatwy LA et al (2021) Greener route for the removal of toxic heavy metals and synthesis of 14-aryl-14H dibenzo[a, j] xanthene using a novel and efficient Ag-Mg bimetallic MOF as a recyclable heterogeneous nanocatalyst. *J Taiwan Inst Chem Eng* 122:176–189
- El-Hakam SA, Samra SE, El-Dafrawy SM et al (2018) Synthesis of sulfamic acid supported on Cr-MIL-101 as a heterogeneous acid catalyst and efficient adsorbent for methyl orange dye. *RSC Adv* 8:20517–20533
- Jia Y, Liu Y, Liu W, Li Z (2014) Study on purification characteristic of CO<sub>2</sub> and CO within closed environment of coal mine refuge chamber. *Sep Purif Technol* 130:65–73

20. James SL (2003) Metal-organic frameworks. *Chem Soc Rev* 32:276–288
21. Abd El Rahman SK, Hassan HMA, El-Shall MS (2012) Acid catalyzed organic transformations by heteropoly tungstophosphoric acid supported on MCM-41. *Appl Catal A* 411:77–86
22. Huckaba CE, Keyes FG (1948) The accuracy of estimation of hydrogen peroxide by potassium permanganate titration. *J Am Chem Soc* 70:1640–1644
23. Liu S, Sun L, Xu F et al (2013) Nanosized Cu-MOFs induced by graphene oxide and enhanced gas storage capacity. *Energy Environ Sci* 6:818–823
24. Mannaa MA, Altass HM, Salama RS (2021) MCM-41 grafted with citric acid: the role of carboxylic groups in enhancing the synthesis of xanthenes and removal of heavy metal ions. *Environ Nanotechnol Monit Manag* 15:100410
25. Salama RS, Hassan SM, Ahmed AI et al (2020) The role of PMA in enhancing the surface acidity and catalytic activity of a bimetallic Cr–Mg-MOF and its applications for synthesis of coumarin and dihydropyrimidinone derivatives. *RSC Adv* 10:21115–21128
26. Abd El Rahman SK, Hassan HMA, El-Shall MS (2014) Metal-organic frameworks with high tungstophosphoric acid loading as heterogeneous acid catalysts. *Appl Catal A* 487:110–118
27. Deng K, Hou Z, Li X et al (2015) Aptamer-mediated up-conversion core/MOF shell nanocomposites for targeted drug delivery and cell imaging. *Sci Rep* 5:7851
28. Ibrahim AA, Salama RS, El-Hakam SA et al (2021) Synthesis of sulfated zirconium supported MCM-41 composite with high-rate adsorption of methylene blue and excellent heterogeneous catalyst. *Colloids Surf A* 616:126361
29. Zhou J, Li R, Fan X et al (2014) Rational design of a metal-organic framework host for sulfur storage in fast, long-cycle Li–S batteries. *Energy Environ Sci* 7:2715–2724
30. El-Shall MS, Abdelsayed V, Abd El Rahman SK et al (2009) Metallic and bimetallic nanocatalysts incorporated into highly porous coordination polymer MIL-101. *J Mater Chem* 19:7625–7631
31. Guo Z, Xiao C, Maligal-Ganesh RV et al (2014) Pt nanoclusters confined within metal-organic framework cavities for chemoselective cinnamaldehyde hydrogenation. *ACS Catal* 4:1340–1348
32. Choi KM, Na K, Somorjai GA et al (2015) Chemical environment control and enhanced catalytic performance of platinum nanoparticles embedded in nanocrystalline metal-organic frameworks. *J Am Chem Soc* 137:7810–7816
33. Li S-L, Xu Q (2013) Metal-organic frameworks as platforms for clean energy. *Energy Environ Sci* 6:1656–1683
34. Fateeva A, Chater PA, Ireland CP et al (2012) A water-stable porphyrin-based metal-organic framework active for visible-light photocatalysis. *Angew Chem Int Ed* 51:7440–7444
35. Kitagawa S, Kitaura R, Noro SI (2004) Functional porous coordination polymers. *Angew Chem Int Ed* 43:2334
36. Zhao Y, Zhong C, Liu C-J (2013) Enhanced CO oxidation over thermal treated Ag/Cu-BTC. *Catal Commun* 38:74–76
37. Ye J, Liu C (2011)  $\text{Cu}_3(\text{BTC})_2$ : CO oxidation over MOF based catalysts. *Chem Commun* 47:2167–2169
38. El-Yazeed WSA, Abou El-Reash YG, Elatwy LA et al (2020) Facile fabrication of bimetallic Fe–Mg MOF for the synthesis of xanthenes and removal of heavy metal ions. *RSC Adv* 10:9693–9703
39. Akyüz G, Elmas A, Andaç M, Andaç Ö (2021) Evaluation of nano sized Mg@BTC metal organic framework as a drug carrier: a long term experimental and predictive theoretical study. *Res Eng Struct Mater* 7:135–156
40. Hassan HMA, Abdelsayed V, Abd El Rahman SK et al (2009) Microwave synthesis of graphene sheets supporting metal nanocrystals in aqueous and organic media. *J Mater Chem* 19:3832–3837
41. Perera SD, Mariano RG, Vu K et al (2012) Hydrothermal synthesis of graphene-TiO<sub>2</sub> nanotube composites with enhanced photocatalytic activity. *ACS Catal* 2:949–956
42. Wang Y, Guo CX, Liu J et al (2011) CeO<sub>2</sub> nanoparticles/graphene nanocomposite-based high performance supercapacitor. *Dalton Trans* 40:6388–6391
43. He Y, Chen W, Li X et al (2013) Freestanding three-dimensional graphene/MnO<sub>2</sub> composite networks as ultralight and flexible supercapacitor electrodes. *ACS Nano* 7:174–182
44. Siamaki AR, Abd El Rahman SK, Abdelsayed V et al (2011) Microwave-assisted synthesis of palladium nanoparticles supported on graphene: a highly active and recyclable catalyst for carbon-carbon cross-coupling reactions. *J Catal* 279:1–11
45. Yoo E, Okata T, Akita T et al (2009) Enhanced electrocatalytic activity of Pt subnanoclusters on graphene nanosheet surface. *Nano Lett* 9:2255–2259
46. Khder AERS, Hassan H, Betiha MA et al (2014) CO oxidation over Au and Pd nanoparticles supported on ceria-hafnia mixed oxides. *React Kinet Mech Catal* 112:61–75
47. Di L, Duan D, Zhang X et al (2016) Effect of TiO<sub>2</sub> crystal phase and preparation method on the catalytic performance of Au/TiO<sub>2</sub> for CO oxidation. *IEEE Trans Plasma Sci* 44:2692–2698
48. Al-Shehri BM, Shkir M, Khder AS et al (2020) Noble metal nanoparticles incorporated siliceous TUD-1 mesoporous nano-catalyst for low-temperature oxidation of carbon monoxide. *Nanomaterials* 10:1067
49. Altass HM, Khder AERS (2018) Catalytic oxidation of carbon monoxide over of gold-supported iron oxide catalyst. *Mater Res Innov* 22:107–114
50. Lestari WW, Tedra RA, Rosari VA, Saraswati TE (2020) The novel composite material MOF-[Mg<sub>3</sub>(BTC)<sub>2</sub>]/GO/Fe<sub>3</sub>O<sub>4</sub> and its use in slow-release ibuprofen. *Appl Organomet Chem* 34:e5670
51. Li X, Odoom-Wubah T, Huang J (2018) Biosynthesis of Ag–Pd bimetallic alloy nanoparticles through hydrolysis of cellulose triggered by silver sulfate. *RSC Adv* 8:30340–30345
52. Altass HM, Abd El Rahman SK (2018) Preparation, characterization of highly active recyclable zirconium and tin tungstate catalysts and their application in Pechmann condensation reaction. *React Kinet Mech Catal* 125:227–243
53. Al-Shehri BM, Khder A-R, Ashour SS et al (2019) Effect of europium loading on the photoluminescence property of europium incorporated 3D-mesoporous silica. *J Non-Cryst Solids* 515:68–74
54. Huang Z, Zhao F, Fan L et al (2020) Improved hydrolytic robustness and catalytic performance of flexible lanthanide-based metal-organic frameworks: a matter of coordination environments. *Mater Des* 194:108881
55. Yang T, Huang L, Harn Y et al (2013) High density unaggregated Au nanoparticles on ZnO nanorod arrays function as efficient and recyclable photocatalysts for environmental purification. *Small* 9:3169–3182
56. Ahmad M, Yingying S, Nisar A et al (2011) Synthesis of hierarchical flower-like ZnO nanostructures and their functionalization by Au nanoparticles for improved photocatalytic and high performance Li-ion battery anodes. *J Mater Chem* 21:7723–7729
57. Wang X, Wang W, Liu Y-L (2012) Enhanced acetone sensing performance of Au nanoparticles functionalized flower-like ZnO. *Sens Actuators B* 168:39–45
58. Zhang J, Liu X, Wu S et al (2012) One-pot synthesis of Au-supported ZnO nanoplates with enhanced gas sensor performance. *Sens Actuators B* 169:61–66
59. Sadri R, Hosseini M, Kazi SN et al (2017) A bio-based, facile approach for the preparation of covalently functionalized carbon nanotubes aqueous suspensions and their potential as heat transfer fluids. *J Colloid Interface Sci* 504:115–123

60. Peng Q, Dai Y, Liu K et al (2020) A novel carbon nanotube–magnesium oxide composite with excellent recyclability to efficiently activate peroxy monosulfate for rhodamine B degradation. *J Mater Sci* 55:11267–11283
61. Surya SG, Bhanoth S, Majhi SM et al (2019) A silver nanoparticle-anchored UiO-66(Zr) metal-organic framework (MOF)-based capacitive H<sub>2</sub>S gas sensor. *CrystEngComm* 21:7303–7312. <https://doi.org/10.1039/c9ce01323g>
62. Hu Z-P, Zhao H, Gao Z-M et al (2016) High-surface-area activated red mud supported Co<sub>3</sub>O<sub>4</sub> catalysts for efficient catalytic oxidation of CO. *RSC Adv* 6:94748–94755
63. Morad M, Karim MA, Altass HM et al (2021) Microwave-assisted synthesis of gold nanoparticles supported on Mn<sub>3</sub>O<sub>4</sub> catalyst for low temperature CO oxidation. *Environ Technol* 42:2680–2689
64. Abd El Rahman SK, Altass HM, Orif MI et al (2019) Preparation and characterization of highly active Pd nanoparticles supported Mn<sub>3</sub>O<sub>4</sub> catalyst for low-temperature CO oxidation. *Mater Res Bull* 113:215–222
65. Han Q, Zhang D, Guo J et al (2019) Improved catalytic performance of Au/α-Fe<sub>2</sub>O<sub>3</sub>-like-worm catalyst for low temperature CO oxidation. *Nanomaterials* 9:1118
66. Zhao Y, Dong F, Han W et al (2019) The synergistic catalytic effect between graphene oxide and three-dimensional ordered mesoporous Co<sub>3</sub>O<sub>4</sub> nanoparticles for low-temperature CO oxidation. *Microporous Mesoporous Mater* 273:1–9
67. Ali AA, Madkour M, Al SF et al (2020) Low-temperature catalytic CO oxidation over non-noble, efficient chromia in reduced graphene oxide and graphene oxide nanocomposites. *Catalysts* 10:105
68. Yan W, Chen Z, Huang J et al (2018) Preparation and catalytic behavior of reduced graphene oxide supported cobalt oxide hybrid nanocatalysts for CO oxidation. *Trans Nonferrous Met Soc China* 28:2265–2273
69. Tanaka S, Lin J, Kaneti YV et al (2018) Gold nanoparticles supported on mesoporous iron oxide for enhanced CO oxidation reaction. *Nanoscale* 10:4779–4785
70. Carabineiro SAC, Bogdanchikova N, Tavares PB et al (2012) Nanostructured iron oxide catalysts with gold for the oxidation of carbon monoxide. *RSC Adv* 2:2957–2965
71. Carabineiro SAC, Bogdanchikova N, Pstryakov A et al (2011) Gold nanoparticles supported on magnesium oxide for CO oxidation. *Nanoscale Res Lett* 6:1–6

**Publisher's Note** Springer Nature remains neutral with regard to jurisdictional claims in published maps and institutional affiliations.

## Authors and Affiliations

Hatem M. Altass<sup>1</sup> · Saleh A. Ahmed<sup>1,2</sup> · Reda S. Salama<sup>3</sup> · Ziad Moussa<sup>4</sup> · Rabab S. Jassas<sup>5</sup> · Reem I. Alsantali<sup>6</sup> · Munirah M. Al-Rooqi<sup>1</sup> · Amr A. Ibrahim<sup>7</sup> · Menna A. Khder<sup>7</sup> · Moataz Morad<sup>1</sup> · Awad I. Ahmed<sup>7</sup> · Abdelrahman S. Khder<sup>1,7</sup> 

<sup>1</sup> Chemistry Department, Faculty of Applied Science, Umm Al-Qura University, Mecca 21955, Saudi Arabia

<sup>2</sup> Chemistry Department, Faculty of Science, Assiut University, Asyût 71516, Egypt

<sup>3</sup> Basic Science Department, Faculty of Engineering, Delta University for Science and Technology, Gamasa, Egypt

<sup>4</sup> Department of Chemistry, College of Science, United Arab Emirates University, P.O. Box 15551, Al Ain, Abu Dhabi, United Arab Emirates

<sup>5</sup> Department of Chemistry, Jamoum University College, Umm Al-Qura University, Mecca 21955, Saudi Arabia

<sup>6</sup> Department of Pharmaceutical Chemistry, College of Pharmacy, Taif University, P.O. Box 11099, Taif 21944, Saudi Arabia

<sup>7</sup> Chemistry Department, Faculty of Science, Mansoura University, Mansoura 35516, Egypt